Supporting Information: Auger Recombination Lifetime Scaling for Type-I and Quasi-Type-II Core/Shell Quantum Dots

John P. Philbin*,† and Eran Rabani*,†,‡,¶

†*Department of Chemistry, University of California, Berkeley, California 94720, United States*

‡*The Sackler Center for Computational Molecular and Materials Science, Tel Aviv University, Tel Aviv, Israel 69978*

¶*Materials Sciences Division, Lawrence Berkeley National Laboratory, Berkeley, California 94720, United States*

E-mail: jphilbin@berkeley.edu; eran.rabani@berkeley.edu

Nanocrystal configurations

The nanostructure configurations were obtained by initially cleaving a sufficiently large wurtzite crystal with a lattice constant of bulk wurtzite CdSe $\left(a = 4.30\,\text{Å},\ c = a\sqrt{\frac{8}{3}}\right)$ such that all Cd, Zn, S and Se atoms have at least two bonds. Because of the lattice mismatch between CdSe and the CdS or ZnS shells, we relaxed the atomic coordinates of the core/shell quantum dots (QDs) prior to performing the electronic structure calculations. Specifically, we utilized molecular dynamics (MD) minimization of the core/shell QDs using the conjugate gradient algorithm. We used LAMMPS with Stillinger–Weber interaction potentials, which were previously developed for Cd, Zn, Se, S heterostructures, to obtain the minimized CdSe/CdS and CdSe/ZnS core/shell QD configurations.[1,2] In the next step, we passivated the

MD minimized structures by using ligand potentials that were taken from Ref. 3. The ligand potentials were placed in the correct location by utilizing the atomic positions of the extra outermost monolayer of Se/S and Cd/Zn atoms and replacing each Se/S (Cd/Zn) atom by a corresponding ligand potential for Cd/Zn (Se/S). Details on the sizes of the core/shell QD configurations are given in Table S1, Table S2, and Table S3.

Table S1: CdSe/CdS QD configuration details. The quantum dots diameters and volumes are given in nm and nm^3, respectively. The CdSe core diameter is 3.8 nm.

Configuration	Shell MLs	Diameter (nm)	Volume (nm^3)
$Cd_{462}Se_{462}$	0	3.8	30.1
$Cd_{462}Se_{462}/Cd_{735}S_{735}$	2	5.4	83.7
$Cd_{462}Se_{462}/Cd_{1326}S_{1326}$	3	6.2	127.2
$Cd_{462}Se_{462}/Cd_{2085}S_{2085}$	4	7.1	183.8
$Cd_{462}Se_{462}/Cd_{3033}S_{3033}$	5	7.9	255.6

Table S2: CdSe/CdS QD configuration details. The quantum dot diameters and volumes are given in nm and nm^3, respectively. The CdSe core diameter is 2.2 nm.

Configuration	Shell MLs	Diameter (nm)	Volume (nm^3)
$Cd_{102}Se_{102}$	0	2.2	5.2
$Cd_{102}Se_{102}/Cd_{120}S_{120}$	1	2.9	13.2
$Cd_{102}Se_{102}/Cd_{333}S_{333}$	2	3.7	27.6
$Cd_{102}Se_{102}/Cd_{651}S_{651}$	3	4.6	49.8
$Cd_{102}Se_{102}/Cd_{1095}S_{1095}$	4	5.4	81.7
$Cd_{102}Se_{102}/Cd_{1686}S_{1686}$	5	6.2	125.1
$Cd_{102}Se_{102}/Cd_{2445}S_{2445}$	6	7.0	181.7
$Cd_{102}Se_{102}/Cd_{4551}S_{4551}$	8	8.7	341.8

Table S3: CdSe/ZnS QD configuration details. The quantum dots diameters and volumes are given in nm and nm^3, respectively. The CdSe core diameter is 2.2 nm.

Configuration	Shell MLs	Diameter (nm)	Volume (nm^3)
$Cd_{102}Se_{102}$	0	2.2	5.2
$Cd_{102}Se_{102}/Zn_{120}S_{120}$	1	2.8	11.7
$Cd_{102}Se_{102}/Zn_{333}S_{333}$	2	3.5	23.3
$Cd_{102}Se_{102}/Zn_{651}S_{651}$	3	4.3	41.1
$Cd_{102}Se_{102}/Zn_{1095}S_{1095}$	4	5.0	66.5
$Cd_{102}Se_{102}/Zn_{1686}S_{1686}$	5	5.8	101.1
$Cd_{102}Se_{102}/Zn_{2445}S_{2445}$	6	6.5	146.2
$Cd_{102}Se_{102}/Zn_{4551}S_{4551}$	8	8.1	273.9

Strained CdSe quantum dot calculations

For the strained CdSe QD nanostructures, MD minimizations were performed with ZnS shells using the aforementioned procedure, and, afterwards, all of the Zn and S atoms were removed from the shell such that the final configuration was that of just the CdSe QD but with strained positions. The results of this procedure for varying amounts of ZnS MLs are shown in Table S4. Because ZnS has a smaller lattice constant than CdSe, the strain is compressive in all dimensions and results in smaller average Cd–Se bonds ($\langle r_{\text{Cd-Se}} \rangle$) and diameters in the strained CdSe QDs relative to the unstrained CdSe QD.

Table S4: Configuration details of the strained CdSe QDs. The quantum dots average Cd–Se bond lengths ($\langle r_{\text{Cd-Se}} \rangle$), diameters, and volumes are given in nm, nm, and nm^3, respectively.

Configuration	ZnS MLs in MD	$\langle r_{\text{Cd-Se}} \rangle$ (nm)	Diameter (nm)	Volume (nm^3)
$Cd_{93}Se_{93}$	0	2.620	2.155	5.242
$Cd_{93}Se_{93}$	1	2.545	2.078	4.702
$Cd_{93}Se_{93}$	2	2.533	2.068	4.634
$Cd_{93}Se_{93}$	4	2.521	2.059	4.569
$Cd_{93}Se_{93}$	8	2.520	2.056	4.552

This procedure allowed us to isolate the impact of the compressive strain, which is induced by the ZnS shell, has on the Auger recombination lifetime (τ_{AR}). Table S5 shows how the addition of the compressive strain results in a reduction of τ_{AR} by about a factor of 2, and the reduction primarily arises from the hole channel. In other words, the Auger recombination channel in which the hole receives a majority of the additional energy ($\tau_{\text{AR,h}}$) becomes faster when the core is compressed. The electron channel lifetime ($\tau_{\text{AR,e}}$) also becomes faster, but not significantly in comparison to the hole channel (Table S5).

Table S5: Auger recombination lifetimes the strained CdSe QDs. The total Auger recombination lifetime (τ_{AR}), Auger recombination lifetime of the hole channel ($\tau_{\text{AR,h}}$), and the Auger recombination lifetime of the electron channel ($\tau_{\text{AR,e}}$) are given in picoseconds (ps).

Configuration	ZnS MLs in MD	τ_{AR} (ps)	$\tau_{\text{AR,h}}$ (ps)	$\tau_{\text{AR,e}}$ (ps)
$Cd_{93}Se_{93}$	0	4.6	8.7	9.8
$Cd_{93}Se_{93}$	1	2.0	3.2	5.5
$Cd_{93}Se_{93}$	2	2.0	3.2	5.7
$Cd_{93}Se_{93}$	4	2.4	3.6	6.9
$Cd_{93}Se_{93}$	8	2.6	3.8	7.6

In order to understand the decrease in the hole channel Auger recombination lifetime, we analyzed the Coulomb matrix elements (V_{ijck}) and number of final states ($n_{\text{h,final}}$) in each of these CdSe QDs in

a noninteracting formalism to simplify the analysis. Interestingly, we found that the major difference arises from an increase in the Coulomb matrix elements (V_{ijck}). Specifically, the average of the square of the Coulomb matrix elements ($\langle V_{ijck}^2 \rangle$) is approximately twice as large in the strained CdSe QDs (bottom four lines in Table S6) compared to the unstrained CdSe QD (top line of Table S6). A similar increase of the Coulomb matrix elements in the electron channel (V_{abck}) is not observed. This suggests that the increase of the Coulomb matrix elements in the hole channel arises from the $\phi_i(\mathbf{r})\,\phi_j(\mathbf{r})$ part of the Eq. (S3) as both the electron and hole channels contain $\phi_c(\mathbf{r}')\,\phi_k(\mathbf{r}')$. The $\phi_i(\mathbf{r})\,\phi_j(\mathbf{r})$ is a product of the initial band–edge hole state ($\phi_j(\mathbf{r})$) with the final high energy hole state ($\phi_i(\mathbf{r})$). We speculate that the compressive strain increases the rate of the hole channel decay by increasing the oscillatory nature of the band–edge hole states, which leads to better overlap with the highly oscillatory final high energy hole states.

Table S6: The number of final high energy hole ($n_{\text{h,final}}$) and electron ($n_{\text{e,final}}$) states that satisfy energy conservation along with the average of the squared Coulomb matrix elements that couple to the high energy hole and electron states, respectively, in a noninteracting Auger recombination lifetime calculation. The average of the squared Coulomb matrix elements is normalized to the unstrained (top line) value.

Configuration	ZnS MLs used in MD	$n_{\text{h,final}}$	Normalized $\langle V_{ijck}^2 \rangle$	$n_{\text{e,final}}$	Normalized $\langle V_{abck}^2 \rangle$
$Cd_{93}Se_{93}$	0	27	1.0	16	1.0
$Cd_{93}Se_{93}$	1	22	2.0	17	1.1
$Cd_{93}Se_{93}$	2	22	2.1	19	1.1
$Cd_{93}Se_{93}$	4	22	2.4	16	1.1
$Cd_{93}Se_{93}$	8	22	2.5	16	1.1

Free carrier states

All calculations were performed within the semi–empirical pseudopotential method for CdSe implemented on real–space grids with spacings of at most 0.8 a.u. – sufficient to converge the results.[3,4] The first step in all of the Auger recombination lifetime formalisms was to apply the filter–diagonalization technique to obtain the band–edge electron and hole states.[5,6] The states obtained from this application of the filter–diagonalization technique were then used to build the initial biexcitonic states in the noninteracting formalism. For the interacting (both stochastic and deterministic formalisms), the band–edge electron and hole states were used as input to the Bethe–Salpeter equation. After solving

the Bethe–Salpeter equation, the initial biexcitonic states can be generated for use in the deterministic and stochastic interacting algorithms. To obtain the final, high energy excitonic states, we again utilized filter–diagonalization techniques to selectively obtain the electron and hole states at energies near resonance with the initial biexcitonic state. Fig. S1 shows the density of states of core/shell QD with a CdSe core diameter of 3.8 nm and 3 MLs of CdS shell to highlight the fundamental gap, density of states at the band–edge, and the density of states an optical gap above the band–edge to explicitly as these are the energies for which the free carrier states need to be calculated in an Auger recombination lifetime calculation.

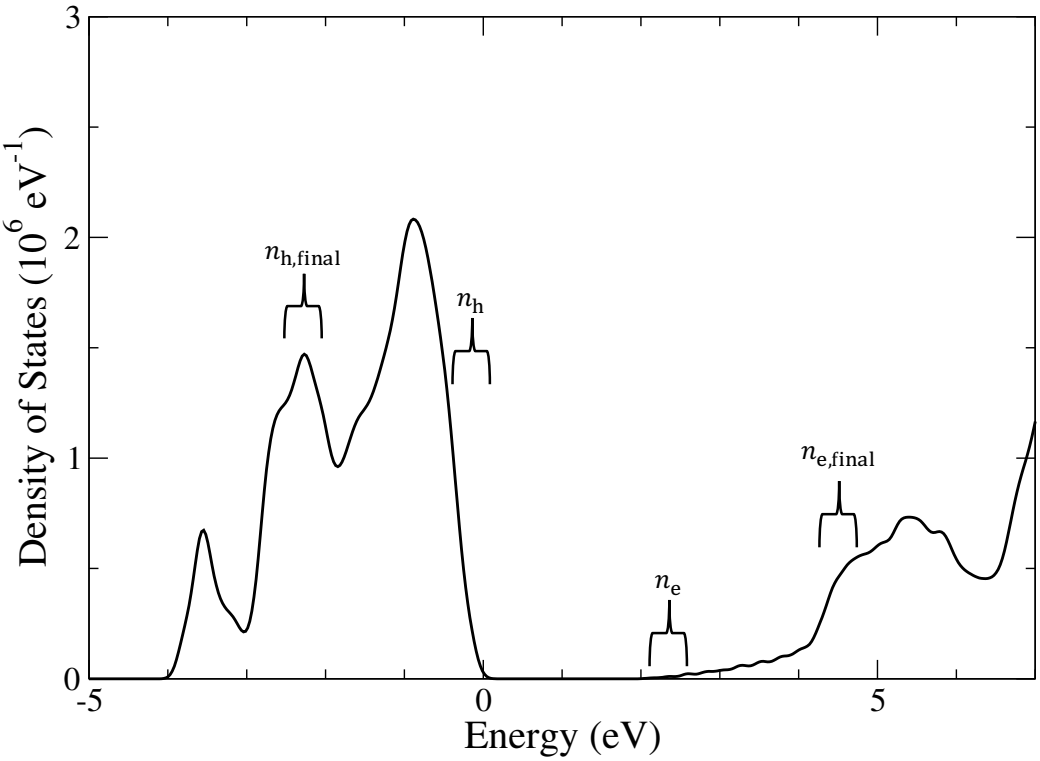

Figure S1: Density of free carrier (i.e. electron and hole) states of a core/shell QD with a CdSe core diameter of 3.8 nm and 3 MLs of CdS shell.

Excitonic states

The correlated electron–hole pair (i.e. excitonic) states used in the initial biexcitonic states in the deterministic and stochastic interacting formalisms were represented using a linear combination of non-interacting electron–hole pairs as discussed briefly in the main text and in detail in Ref. 7. The electron–

hole kernel in the Bethe–Salpeter equation included both the screened direct Coulomb attraction and exchange–like repulsive term, as the latter term is needed for bright excitons (i.e., excitons generated by a photon absorption) in core/shell QDs.[7] The charge carrrier densities of the lowest excitonic state for a CdSe core diameter of 2.2 nm and 8 MLs of CdS shell is shown in Fig. S2.

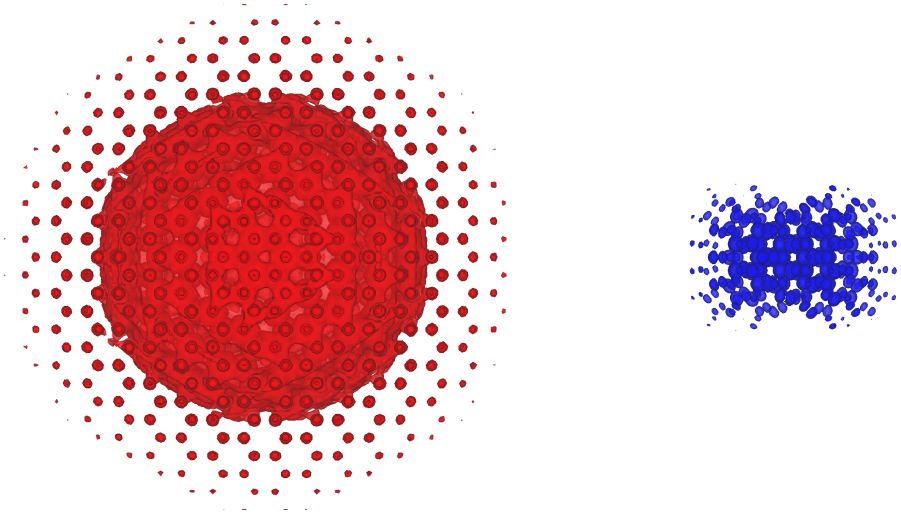

Figure S2: Charge carrier densities for the lowest energy excitonic state for the electron (left, red) and hole (right, blue) for a CdSe core diameter of 2.2nm and 8 MLs of CdS shell. The electron carrier density is shown to approximately be a linear combination of S–like atomic orbitals whereas the hole carrier density is shown to approximately be a linear combination of P–like atomic orbitals. The localization of the hole to the CdSe core is shown by its smaller spatial extent compared to the electron density.

Energy conservation in Fermi's golden rule

We enforced conservation of energy ($\delta\left(E_B - E_S\right)$) in Fermi's golden rule by approximating the delta function as:

$$\delta\left(x\right) = \begin{cases} \frac{1}{2dE} & -dE < x < dE \\ 0 & \text{otherwise} \end{cases}, \tag{S1}$$

where dE is a parameter (i.e. all final single excitonic states with energies between $E_B \pm dE$ were taken to conserve energy). We reported AR lifetimes for $dE \approx 20$ meV – similar broadening to what was used in previous calculations.[8,9] Importantly, the conclusions discussed in the main text do not change for dE values ranging from $5 - 50$ meV.

Details of the Auger recombination formalisms

A few useful definitions for analyzing the computational cost are:

$$
\begin{aligned}
N_{\text{grid}} &\equiv \text{number of grid points} \\
N_{\text{e}} &\equiv \text{number of band–edge electrons used in the Bethe-Salpeter equation (b,c states)} \\
N_{\text{h}} &\equiv \text{number of band–edge holes used in the Bethe-Salpeter equation (j,k states)} \\
N_{\text{e,final}} &\equiv \text{number of high energy electrons satisfying energy conservation (a states)} \\
N_{\text{h,final}} &\equiv \text{number of high energy holes satisfying energy conservation (i states)} \\
N &\equiv \text{measure of the overall system size.}
\end{aligned}
$$

Deterministic Auger recombination lifetime formalism

As discussed in the main text and in our previous work in detail,[9] the expression for calculating an Auger recombination (AR) lifetime (τ_{AR}) in the interacting formalism is

$$
\begin{aligned}
\tau_{\text{AR}}^{-1} &= \frac{2\pi}{\hbar Z_B} \sum_B e^{-\beta E_B} \sum_{a,i} \left| \sum_{b,c,k} c_{b,i}^B c_{c,k}^B V_{abck} \right|^2 \delta\left(E_B - \varepsilon_a + \varepsilon_i\right) \\
&\quad + \frac{2\pi}{\hbar Z_B} \sum_B e^{-\beta E_B} \sum_{a,i} \left| \sum_{j,c,k} c_{a,j}^B c_{c,k}^B V_{ijck} \right|^2 \delta\left(E_B - \varepsilon_a + \varepsilon_i\right), \qquad \text{(S2)}
\end{aligned}
$$

where V_{rsut} is the Coulomb coupling given by

$$
V_{rsut} = \iint \frac{\phi_r\left(\mathbf{r}\right) \phi_s\left(\mathbf{r}\right) \phi_u\left(\mathbf{r}'\right) \phi_t\left(\mathbf{r}'\right)}{|\mathbf{r} - \mathbf{r}'|} d^3\mathbf{r}\, d^3\mathbf{r}', \qquad \text{(S3)}
$$

the coefficients ($c_{c,k}^B$) in Eq. (S2) are determined by solving the Bethe–Salpeter equation,[7] and $\phi_r\left(\mathbf{r}\right)$ are quasiparticle states for electrons ($r \in a, b, c, ..$) or holes ($r \in i, j, k, ...$).

Computational cost of main text Eq. (2)

We will now break down the computational scaling of Eq. (S2) in detail. (As discussed in the main text, we assume the Bethe–Salpeter equation has already been solved.) The main difficulty and current

computational bottleneck in Eq. (S2) is calculating all of the Coulomb matrix elements (V_{abck} and V_{ijck}) that couple the initial biexcitonic states with the final electron–hole pairs in large nanomaterials (e.g. core/shell QDs). Specifically, the number of Coulomb matrix elements that must be calculated scales as $O\left(N_{\mathrm{e,final}}N_{\mathrm{e}}^{2}N_{\mathrm{h}}+N_{\mathrm{h,final}}N_{\mathrm{h}}^{2}N_{\mathrm{e}}\right)\sim O\left(N^{4}\right)$, where $N_{\mathrm{e(h),final}}$ is the number of high energy final electron (hole) states and $N_{\mathrm{e(h)}}$ is the number of band–edge electron (hole) states, and the cost of calculating each Coulomb matrix element scales with the number of real–space grid points (N_{grid}) as $O\left(N_{\mathrm{grid}}\ln N_{\mathrm{grid}}\right)$ using fast Fourier transforms. This gives the overall scaling of Eq. (S2) as

$$\tau_{\mathrm{AR}}^{-1}\;\sim\;O\left(N_{\mathrm{e,final}}N_{\mathrm{e}}^{2}N_{\mathrm{h}}N_{\mathrm{grid}}\ln N_{\mathrm{grid}}\right)+O\left(N_{\mathrm{h,final}}N_{\mathrm{h}}^{2}N_{\mathrm{e}}N_{\mathrm{grid}}\ln N_{\mathrm{grid}}\right). \tag{S4}$$

This limits the application of Eq. (S2) to relatively small systems ($\leq 1,000$ atoms). In terms of the overall system size (N), Eq. (S2) scales as $O\left(N^{5}\ln N\right)$ which approaches $O\left(N^{5}\right)$ as N approaches infinity.

Stochastic Auger recombination lifetime formalisms

Computational cost of main text Eq. (7)

The computational scaling of main text Eq. (7) arises from the calculation of the R_{rs}^{ζ} matrices,

$$R_{rs}^{\zeta}\;=\;\int\phi_{r}^{*}\left(\mathbf{r}\right)\phi_{s}^{*}\left(\mathbf{r}\right)\theta^{\zeta}\left(\mathbf{r}\right)\,d^{3}\mathbf{r}, \tag{S5}$$

where $\theta^{\zeta}\left(\mathbf{r}\right)$ is a stochastic orbital indexed by ζ and described in detail in the main text. Specifically, the three matrices that must be calculated are R_{ck}^{ζ}, R_{ab}^{ζ}, and R_{ij}^{ζ}. The number of matrix elements is $N_{r}N_{s}N_{\zeta}$, where N_{ζ} is the number of stochastic orbitals. Because each matrix element is just a simple 3D integral, the cost of calculating a single matrix element is just N_{grid}. Fortunately, N_{ζ} does not increase with system size.[10–13] Thus, the computational cost of main text Eq. (7) is

$$
\begin{aligned}
\tau_{\mathrm{AR}}^{-1} &\sim O\left(R_{ck}^{\zeta}\right) + O\left(R_{ab}^{\zeta}\right) + O\left(R_{ij}^{\zeta}\right) \\
\tau_{\mathrm{AR}}^{-1} &\sim O\left(N_{\mathrm{e}} N_{\mathrm{h}} N_{\mathrm{grid}}\right) + O\left(N_{\mathrm{e}} N_{\mathrm{e,final}} N_{\mathrm{grid}}\right) + O\left(N_{\mathrm{h}} N_{\mathrm{h,final}} N_{\mathrm{grid}}\right) \\
\tau_{\mathrm{AR}}^{-1} &\sim O\left(N^3\right). \qquad \text{(S6)}
\end{aligned}
$$

Convergence of of main text Eq. (7)

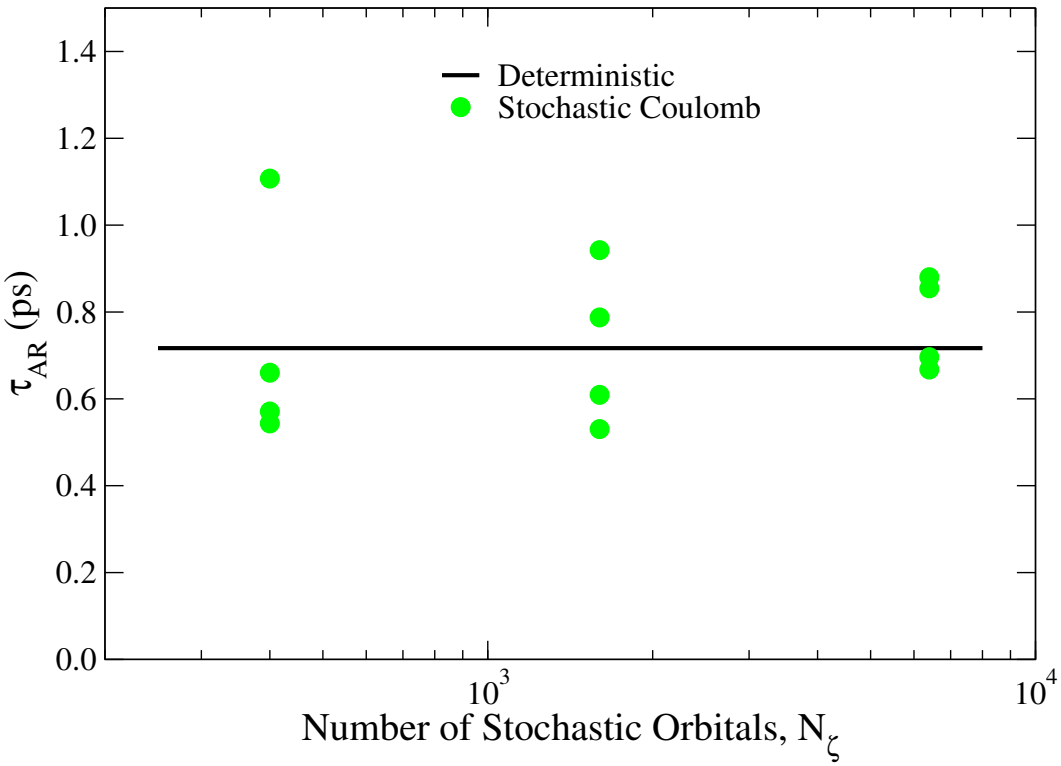

Figure S3: Comparison of the Auger recombination lifetime (τ_{AR}) calculated using main text Eq. (7) and main text Eq. (2) for a small CdSe QD ($Cd_{19}Se_{20}$, diameter = 1.2 nm).

Sampling the final states

Because $N_{\mathrm{e,final}}$ and $N_{\mathrm{h,final}}$ become large ($> 1,000$) for large NCs (e.g. core/shell QDs), we avoid having to calculate R_{ab}^{ζ} and R_{ij}^{ζ} for all of the final high energy electron (a) and hole (i) states by sampling the final states. Specifically, we avoid this rate limiting step in the calculations by forming random linear combinations of the final, high energy electron ($\left|\theta^A\right\rangle$) and hole ($\left|\theta^I\right\rangle$) states for the electron and hole

channels, respectively,

$$\left|\theta^A\right\rangle = \sum_a^{N_{\text{e,final}}} c_a \left|a\right\rangle \tag{S7}$$

$$\left|\theta^I\right\rangle = \sum_i^{N_{\text{h,final}}} c_i \left|i\right\rangle . \tag{S8}$$

The coefficients c_a (c_i) are randomly chosen such that the stochastic orbitals ($\left|\theta^A\right\rangle$ and $\left|\theta^I\right\rangle$) obey the stochastic resolution of the identity[12,13] within their respective subspaces of the Hamiltonian

$$\hat{1}_{\text{e,final}} \approx \left\langle \left|\theta^A\right\rangle \left\langle\theta^A\right| \right\rangle_A \tag{S9}$$

$$\hat{1}_{\text{h,final}} \approx \left\langle \left|\theta^I\right\rangle \left\langle\theta^I\right| \right\rangle_I . \tag{S10}$$

Computational cost of main text Eq. (8)

Main text Eq. (8) has a reduced computational scaling compared to main text Eq. (7) because the summations over the final single excitonic state ($\sum_{a,i}$) have been replaced by averages over stochastic orbitals ($\left|\theta^A\right\rangle$ and $\left|\theta^I\right\rangle$). This reduces the computational scaling from $O\left(N^3\right)$ to $O\left(N^2\right)$ as $N_{\text{e,final}}$ and $N_{\text{h,final}}$ no longer increase with the system size.

Convergence main text Eq. (8)

Table S7: Comparison of the Auger recombination lifetime (τ_{AR}) calculated using main text Eq. (2), main text Eq. (7), and main text Eq. (8) for a CdSe QD (diameter = 4.0 nm). The number of stochastic orbitals used to represent the Coulomb operator (N_ζ) along with the number of stochastic orbitals used to sample the final electron (N_{A}) and hole (N_{I}) states.

Configuration	Main Text Equation	N_ζ	N_{A}	N_{I}	τ_{AR} (ps)
$Cd_{525}Se_{525}$	Eq. (2)	-	-	-	64
$Cd_{525}Se_{525}$	Eq. (7)	6400	-	-	65
$Cd_{525}Se_{525}$	Eq. (7)	6400	-	-	68
$Cd_{525}Se_{525}$	Eq. (8)	6400	400	400	66

References

(1) Plimpton, S. Fast Parallel Algorithms for Short-Range Molecular Dynamics. *J. Comput. Phys.* **1995**, *117*, 1–19.

(2) Zhou, X. W.; Ward, D. K.; Martin, J. E.; Van Swol, F. B.; Cruz-Campa, J. L.; Zubia, D. Stillinger-Weber Potential for the II-VI Elements Zn-Cd-Hg-S-Se-Te. *Phys. Rev. B* **2013**, *88*, 085309.

(3) Rabani, E.; Hetenyi, B.; Berne, B. J.; Brus, L. E. Electronic Properties of CdSe Nanocrystals in the Absence and Presence of a Dielectric Medium. *J. Chem. Phys.* **1999**, *110*, 5355–5369.

(4) Wang, L.-W.; Zunger, A. Pseudopotential Calculations of Nanoscale CdSe Quantum Dots. *Phys. Rev. B* **1996**, *53*, 9579–9582.

(5) Wall, M. R.; Neuhauser, D. Extraction, Through Filter-diagonalization, of General Quantum Eigenvalues or Classical Normal Mode Frequencies from a Small Number of Residues or a Short-time Segment of a Signal. I. Theory and Application to a Quantum-dynamics Model. *J. Chem. Phys.* **1995**, *102*, 8011–8022.

(6) Toledo, S.; Rabani, E. Verly Large Electronic Structure Calculations using an Out-of-core Filter-diagonalization Method. *J. Comput. Phys.* **2002**, *180*, 256–269.

(7) Rohlfing, M.; Louie, S. G. Electron-hole Excitations and Optical Spectra From First Principles. *Phys. Rev. B* **2000**, *62*, 4927–4944.

(8) Wang, L.-W.; Califano, M.; Zunger, A.; Franceschetti, A. Pseudopotential Theory of Auger Processes in CdSe Quantum Dots. *Phys. Rev. Lett.* **2003**, *91*, 056404.

(9) Philbin, J. P.; Rabani, E. Electron-Hole Correlations Govern Auger Recombination in Nanostructures. *Nano Lett.* **2018**, *18*, 7889–7895.

(10) Baer, R.; Rabani, E. Expeditious Stochastic Calculation of Multiexciton Generation Rates in Semiconductor Nanocrystals. *Nano Lett.* **2012**, *12*, 2123–2128.

(11) Baer, R.; Neuhauser, D.; Rabani, E. Self-averaging Stochastic Kohn-Sham Density-functional Theory. *Phys. Rev. Lett.* **2013**, *111*, 106402.

(12) Takeshita, T. Y.; Jong, W. A. D.; Neuhauser, D.; Baer, R.; Rabani, E. Stochastic Formulation of the Resolution of Identity: Application to Second Order Møller-Plesset Perturbation Theory. *J. Chem. Theory Comput.* **2017**, *13*, 4605–4610.

(13) Dou, W.; Takeshita, T. Y.; Chen, M.; Baer, R.; Neuhauser, D.; Rabani, E. Stochastic Resolution of Identity for Real-Time Second-Order Green's Function: Ionization Potential and Quasi-Particle Spectrum. *J. Chem. Theory Comput.* **2019**, *15*, 6703–6711.